Journal of Materials Chemistry

www.rsc.org/materials

Volume 20 | Number 14 | 14 April 2010 | Pages 2693–2896

ISSN 0959-9428

RSC Publishing

Fabrication of long TiO_2 nanotube arrays in a short time using a hybrid anodic method for highly efficient dye-sensitized solar cells†

Lu-Lin Li,[a] Chiau-Yiag Tsai,[a] Hui-Ping Wu,[a] Chien-Chon Chen[b] and Eric Wei-Guang Diau*[a]

Received 20th October 2009, Accepted 18th December 2009
First published as an Advance Article on the web 1st February 2010
DOI: 10.1039/b922003h

We report a simple hybrid anodic method, with initial potentiostatic anodization followed by galvanostatic anodization, to grow much longer titania nanotube (TNT) arrays in a much shorter anodization period (t). The length of the TNT arrays (L) depends linearly on t and is controlled by the electric current; the growth rates are 5.3, 10.7 and 20.3 μm h^{-1} for current densities 3.7, 5.6 and 7.5 mA cm^{-2}, respectively. The produced TNT films of $L = 15$–57 μm sensitized with N719 dye were fabricated into devices for photovoltaic characterization. The NT-DSSC devices show systematically improved cell performance depending on L, reflecting the excellent intrinsic light-scattering property of the NT-DSSC devices to harvest increased sunlight with long TNT arrays. The great effective surface area inside TNT arrays has been shown to significantly increase the dye loading, which might help to enhance the cell performance of the device with co-sensitizing of different dyes for improved efficiency of light harvesting in the future. The best performance of the NT-DSSC device was achieved at $L \sim 30$ μm with a spacer of similar thickness, giving $J_{SC} = 14.63$ mA cm^{-2}, $V_{OC} = 0.741$ V, $FF = 0.70$, and $\eta = 7.6\%$, which is unprecedented for a back-illumination DSSC.

Introduction

Dye-sensitized solar cells (DSSC) have received much attention because of global warming and the demand for cheap sources of renewable energy.[1] The electron-collecting layer of a DSSC is composed of randomly packed TiO_2 nanoparticles (NP) and the best efficiency (η) of power conversion of a NP-DSSC device has attained $\eta \sim 11\%$.[2–6] The great advantage of a NP-DSSC is the large surface area of the nanoporous TiO_2 films for dye adsorption, but the trap-limited diffusion for electron transport in NP-DSSC limits the efficiency.[7–10] To improve the efficiency of charge collection by promoting rapid electron transport and slow charge recombination, vertically oriented arrays of one-dimensional TiO_2 nanotubes have been prepared using potentiostatic anodization[9–17] as a promising advance in DSSC applications.[13–19]

Even though the TNT arrays have the advantage of greater efficiency of charge collection and light scattering superior to their NP-based counterparts,[10] production of long tubes requires prolonged anodization. For instance, Zhu *et al.*[10] fabricated TNT arrays of length (L) 5.7 μm in a glycerol electrolyte containing 0.5% NH_4F at a bias voltage of 20 V for 70 h; Shankar *et al.*[13] fabricated TNT arrays (L = 20 μm) in an electrolyte comprising 8 wt % *tert*-butyl ammonium fluoride in formamide at 20 V for 24 h; Chen *et al.*[15] produced TNT arrays (L = 19 μm) in an ethylene glycol (EG) electrolyte containing 0.5% NH_4F at 60 V for 3 h. In the latter two cases, the cell performances of the corresponding NT-DSSC devices attained $\eta \sim 7\%$ at $L \sim 20$ μm with $TiCl_4$ post-treatment under rear illumination. Based on intensity-modulated photocurrent and photovoltage measurements, Jennings *et al.*[20] determined the diffusion length of a NT-DSSC device to be 100 μm, which is three times that of a typical NP-DSSC device. This information indicates that the performance of a NT-DSSC might be improved if longer TNT arrays can be fabricated for the device. Unfortunately, experimental data on photovoltaic performance of a NT-DSSC device with L longer than 30 μm were not available due to the technical difficulties introduced below.

With the traditional potentiostatic anodization, long TNT arrays might be produced at increased concentrations of fluoride or at greater applied bias voltages with long duration of anodization, but pore clogging increases with increasing F^- concentration because of chemical dissolution at the TiO_2/electrolyte interface; a large bias voltage might produce cracking of the films so that they become easily peeled from the Ti substrate.[15,21] From a technical point of view, during potentiostatic anodization the current density rapidly decreases from a large initial value because an insulating oxide layer is formed on the Ti surface.[11,13,22,23] The decreased current density significantly diminishes the rate of growth (v) of the tube and thus limits growing a long TNT array in a brief duration. To remedy this problem, we designed a hybrid anodic method (Scheme 1) using a combined potentiostatic (constant-voltage) and galvanostatic (constant-current) approach to grow a TNT array as long as ~70 μm firmly on a Ti substrate with an anodization period as small as ~4 h. The TNT films produced with L = 15–57 μm were fabricated into devices that exhibit an excellent light-harvesting efficiency of NT-DSSC through the intrinsic light-scattering effect of devices with longer tubes.

[a]*Department of Applied Chemistry, Institute of Molecular Science, National Chiao Tung University, No.1001, Ta Hsueh Rd., Hsinchu 30010, Taiwan. E-mail: diau@mail.nctu.edu.tw; Fax: +886-3-5723764; Tel: +886-3-5131524*
[b]*Department of Energy and Resources, National United University, 1, Lienda, Miaoli, 36003, Taiwan*

† Electronic supplementary information (ESI) available: SEM side-view images to determine the length of the TNT arrays, the absorption spectra of the dye-loading experiments, and details of the integrated photocurrent densities of NT-DSSC devices to estimate J_{SC}. See DOI: 10.1039/b922003h

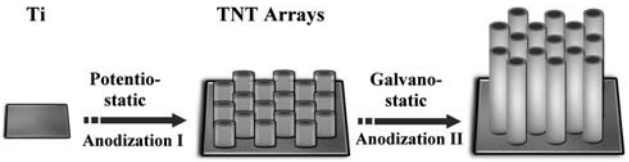

Scheme 1 A hybrid anodic method showing the growth of TNT arrays on Ti foil in two consecutive steps.

Experimental section

Fabrication of TNT arrays

We used Ti foil (commercially pure grade 1, 99.9% purity, Kobe steel) substrate (size 6 × 6 cm^2) as anodes to grow TNT arrays; the cathode was another Ti foil of the same size and the two electrodes were separated by 2.7 cm in a thermostatic container (T = 25 °C) containing the electrolyte solution for anodization. The ordered TNT films were produced in electrolyte solutions containing ammonium fluoride (NH_4F, 99.9%, 0.4 wt %) in EG in the presence of H_2O (2 vol %) *via* the two-step hybrid anodic method, *i.e.*, an initial constant-voltage anodization followed by constant-current anodization. After this process, the anodic sample was washed in ethanol, and annealed at 450 °C for 1 h to crystallize amorphous TiO_2 into its anatase phase. To obtain TNT arrays free of debris for DSSC applications, the annealed sample was then ultrasonicated in ethanol for 15 min to remove the bundled impurities on the top openings of the pores of the nanotubes.

$TiCl_4$ post-treatment

The TNT films were treated with $TiCl_4$ with a two-stage procedure described elsewhere.[15] For the first treatment, the films were immersed in $TiCl_4$ (0.073 M, 30 min) followed by appropriate rinsing and drying at 23 °C; for the second treatment, the films were immersed in $TiCl_4$ (0.073 M, 1 h) again and annealed at 350 °C for 30 min. The surface morphology of the TNT arrays was determined with a scanning electron microscope (SEM, JSM-6500F JEOL).

Device fabrication

We immersed the TNT films (0.5 × 0.5 cm^2) in a solution of N719 dye (3 × 10^{-4} M, Solaronix) containing chenodeoxycholic acid (CDCA, 3 × 10^{-4} M) in acetonitrile/*tert*-butanol (1 : 1 v/v) binary solvent for 24 h to absorb sufficient N719 dye for light harvesting. The samples were then washed with ethanol to remove the remaining dye. To fabricate a NT-DSSC device, the N719/TNT film served as an anode combined with a transparent Pt counter electrode that served as a cathode. The cathode was made by spin-coating a H_2PtCl_6/isopropanol solution on an indium-doped tin-oxide (ITO; 2.8 Ω/sq) glass substrate (typical size 1.0 × 1.5 cm^2) through thermal decomposition at 380 °C for 30 min.[24] The NT-DSSC device was simply sealed with a hot-molten film (SX1170, Solaronix, thickness 60 μm for most cases and 30 μm for the optimization case with L = 30 μm); a thin layer of electrolyte was introduced into the space between the two electrodes. A typical electrolyte contained lithium iodide (LiI, 0.1 M), diiodine (I_2, 0.01 M), 4-*tert*-butylpyridine (TBP, 0.5 M), butyl methyl imidazolium iodide (BMII, 0.6 M), and guanidinium thiocyanate (GuNCS, 0.1 M) in a mixture of acetonitrile (CH_3CN, 99.9%) and valeronitrile (n-C_4H_9CN, 99.9%) (v/v = 85/15).

Dye-loading examination

To determine the dye-loading amount of the N719/TNT films, the dye was desorbed in NaOH aqueous solution (2 mL, 0.1 M).[25] The absorption spectrum of the aqueous solution was recorded with a spectrometer (Varian, Cary 50). A calibration curve for N719 in NaOH/H_2O solution was prepared to obtain the absorption coefficient, 10690 M^{-1} cm^{-1} at 500 nm. The amounts of dye coverage on TNT films shown in the third column of Table 1 were obtained from the measured absorbances of the spectra at 500 nm (cuvette thickness 1 mm) and the calibrated absorption coefficient of N719 according to Beers' law.

Device characterization

The current–voltage characteristics were measured with a digital source meter (Keithley 2400, computer-controlled) with the device under one-sun AM-1.5 irradiation from a solar simulator (SAN-EI, XES-502S) calibrated with a standard silicon reference cell (VLSI standards, Oriel PN 91150V). The NT-DSSC devices were operated with rear illumination and the transparent counter electrode was masked with a black plastic tape of the same size of anode to ensure the same actively illuminated area, 0.25 cm^2, for all measurements. The spectra of the efficiency of conversion of incident photons to current (IPCE) of the corresponding devices were obtained with a system[15] containing a Xe lamp (PTi A-1010, 150 W), a monochromator (Dongwoo DM150i, 1200 gr/mm blazed at 500 nm), and a source meter (Keithley 2400).

Results and discussion

Fabrication of TNT arrays using hybrid anodic method

The purpose of using the proposed hybrid anodic method is to have a good TNT pattern on Ti foil using the potentiostatic approach in the first step, and then switch to the galvanostatic approach for growing long TNT arrays in a brief duration in the second step (Scheme 1). To demonstrate the advantage of our hybrid method superior to the conventional potentiostatic approach, we have carried out control experiments to find the best conditions for growing the TNT films using the hybrid method introduced herein. Fig. 1a–c show the variations of voltage, current and impedance, respectively, as a function of

Table 1 Amounts of loaded dye and the corresponding photovoltaic parameters of NT-DSSC devices as a function of tube length (L) under simulated AM-1.5 illumination (power 100 mW cm^{-2}) and active area 0.25 cm^2. The results of $TiCl_4$ post-treated NT-DSSC devices are shown in parentheses

t/h	L/μm	Dye loading /nmol cm^{-2}	J_{SC}/mA cm^{-2}	V_{OC}/V	FF	η/%
1.5	15	97 (107)	8.6 (10.7)	0.78 (0.76)	0.67 (0.65)	4.5 (5.3)
2	20	108 (130)	10.2 (11.3)	0.75 (0.76)	0.66 (0.66)	5.1 (5.6)
3	32	157 (256)	11.3 (13.6)	0.74 (0.73)	0.66 (0.67)	5.5 (6.6)
4	43	255 (345)	12.9 (14.3)	0.73 (0.72)	0.64 (0.67)	6.0 (6.9)
5	57	312 (441)	13.6 (14.5)	0.70 (0.73)	0.64 (0.64)	6.1 (6.7)

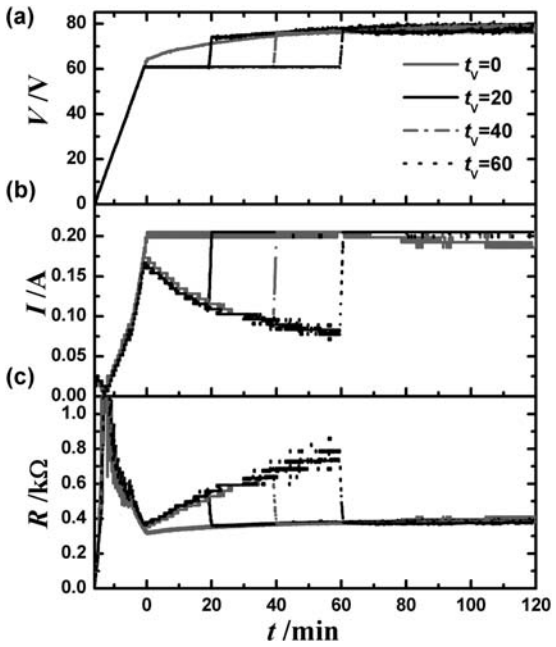

Fig. 1 The anodic variations of (a) voltage (V/V), (b) current (I/A) and (c) impedance (R/kΩ) as a function of anodization period (t/min) showing curves with different constant voltage durations: t_V/min = 0 (grey solid); 20 (black solid); 40 (grey dash-dotted); 60 (black dotted).

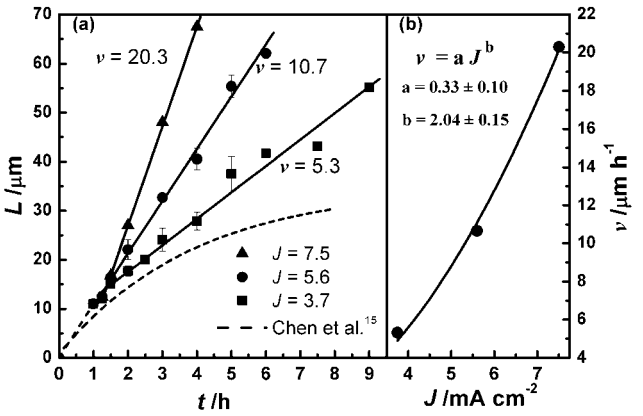

Fig. 2 (a) The tube length (L) as a function of anodization period (t) obtained from the hybrid anodic method (t_V = 1 h) at the current densities (J/mA cm^{-2}) of 3.7 (■), 5.6 (●), and 7.5 (▲), in comparison with the results obtained from a typical potentiostatic method (dashed curve).[15] The corresponding SEM images are shown in Fig. S1–S3 (ESI). The tube growing rates (v/μm h^{-1}) exhibit a linear relationship for all three current densities with the slopes as indicated. (b) The growth rates (v) as a function of the anodization current densities (J) showing a quadratic relation according to the equation $v = aJ^b$.

anodization period (t) in three stages. In the first stage, the bias voltage was gradually increased to 60 V during 15 min (Fig. 1a); only an anodic pitting pattern of the tubes was formed in this stage. The current (I) was increased to 0.19 A (current density J = 5.2 mA cm^{-2}) at the end of this stage (Fig. 1b); we define the initiation of anodization at this point (t = 0). In the second stage, the voltage was kept at 60 V for a short duration t_V which is variable from 0–60 min; this stage is the same as that of a typical potentiostatic anodization applied elsewhere,[13–23] but in this stage we expect to produce a good "template" for the use of growing longer tubes in a smaller duration followed by a galvanostatic approach.

Because the impedance of the anode increased as the TNT arrays grew (Fig. 1c), the current decreased upon anodization under a constant-voltage condition (Fig. 1b). The third stage began at $t = t_V$; the condition of constant voltage was quickly switched to a condition of constant current with current density fixed at 5.6 mA cm^{-2} (I = 0.2 A). When this proceeded, we found that the voltage kept on increasing to reach equilibrium with longer durations for the cases of t_V = 0 and 20 min, while the voltage variations were much less for the cases of t_V = 40 and 60 min (Fig. 1a). The system was particularly stable with better tube growth conditions at t_V = 1 h, for this reason we chose this hybrid condition throughout all the experiments reported herein.

When the galvanostatic anodization proceeded from t_V = 1 h, the voltage initially decayed but attained a steady state in ~30 min because of the suddenly increased voltage. The anodization then progressed smoothly as the voltage gradually increased to maintain the current constant. Additionally, in this stage the impedance of the system varies only slightly so that the growth rate of the TNT arrays can be well controlled. Fig. 2a shows the tube length as a function of anodization duration using our hybrid anodic method in comparison with the results obtained from the potentiostatic method (dashed curve).[15] For TNT arrays grown at constant voltage 60 V, the length of the tubes increased asymptotically with increasing anodization period to $L \sim 30$ μm at t = 8 h; to grow longer TNT arrays required a much greater duration because the anodization current decayed severely under the potentiostatic condition (Fig. 1b). For TNT arrays grown under a constant current density of 5.6 mA cm^{-2}, the length increased linearly to reach $L \sim 60$ μm at t = 6 h. The data of L *vs.* t were fitted satisfactorily with a straight line with a slope v = 10.7 μm h^{-1} for t/h = 1.5–6.0; the data for t/h = 1.0–1.5 were not used for the fit because the applied voltage has not reached a steady state during that period (Fig. 1a). For TNT arrays grown under constant current densities of 3.7 and 7.5 mA cm^{-2}, the growth rates (v) were 5.3 and 20.3 μm h^{-1}, respectively. The rate of tube growth thus quadrupled when the current density was doubled, showing a quadratic relationship according to the equation $v = a\,J^b$ with $b = 2.04 \pm 0.15$ (Fig. 2b). The growth rate is thus proportional to the electric power consumed during the galvanostatic anodization ($v \propto w_{elec} = I^2R$). Our results demonstrate the concept of field-assisted oxidation at an interface between Ti and TNT arrays in a galvanostatic approach to be driven by the current density rather than the potential of the system.

Length-dependent photovoltaic performance

Our results indicate that the surfaces of the TNT films are covered with unwanted clumps that clog the entrances of the tubes. After sonication to remove the undesired surface debris and the porous part of the TNT arrays, the tube lengths at each anodization period were determined from the corresponding SEM side-view images (Figs. S1–S3, ESI). We therefore selected five anodic TNT films of various tube lengths to assess their photovoltaic properties: the tube lengths were 15, 20, 32, 43 and 57 μm produced *via* hybrid anodization at growth current density 5.6 mA cm^{-2} with

t/*h* = 1.5, 2, 3, 4 and 5, respectively; the corresponding SEM images are shown in Fig. 3a–e. The current–voltage characteristics of the NT-DSSC devices fabricated using these TNT films are shown in Fig. 4a and b for those without and with $TiCl_4$ post-treatment, respectively. We summarize the corresponding photovoltaic parameters in Table 1, which demonstrates that the current density at short circuit (J_{SC}/mA cm^{-2}), the voltage at open circuit (V_{OC}/V), the filling factor (*FF*), and the efficiency ($\eta = J_{SC}V_{OC}FF/P_{in}$ with $P_{in} = 100$ mW cm^{-2}) of power conversion vary as a function of the tube length. For the devices without $TiCl_4$ treatment, the results display a systematic trend for J_{SC}, in which the current density significantly increases from $J_{SC} = 8.6$ mA cm^{-2} at $L = 15$ μm to $J_{SC} = 13.6$ mA cm^{-2} at $L = 57$ μm. The results are consistent with those obtained from a potentiostatic experiment sensitized with the N3 dye in which $J_{SC} = 10.0$ mA cm^{-2} at $L = 14$ μm and $J_{SC} = 12.5$ mA cm^{-2} at $L = 30$ μm.[15]

The dye-loading experiments (Fig. S4, ESI) disclose the amount of dye molecules adsorbed inside the TNT arrays (Table 1), and confirmed that longer tubes offer a larger surface area on which dye molecules adsorb. Our results show also a systematic trend for both V_{OC} and *FF* decreasing with increasing tube length. Because the extent of the increase of J_{SC} was much greater than the extent of the decrease of V_{OC} and *FF*, the overall cell performance exhibited a systematic increase: η (%) = 4.5, 5.1, 5.5, 6.0 and 6.1 with L/μm = 15, 20, 32, 43 and 57, respectively. The cell performances hence seem to balance between J_{SC} and V_{OC} for the two long tubes (L = 43 and 57 μm), so that their efficiencies of power conversion are similar. For the devices treated with $TiCl_4$, the effective surface areas for dye loading were further enhanced, yielding a significantly increased J_{SC} (Table 1 in parentheses). The cell performances increased from η = 5.3% at L = 15 μm to η = 6.9% at L = 43 μm, but the performance decreased slightly to η = 6.7% at L = 57 μm.

Light-scattering effect on tube length

Fig. 5a and b show action spectra for the incident photon-to-current conversion efficiency (IPCE) of five NT-DSSC devices

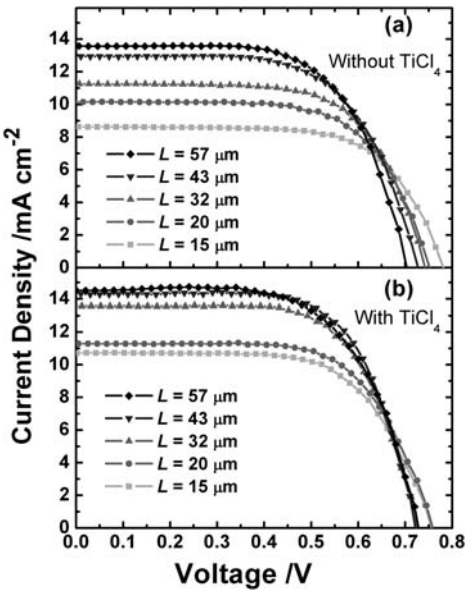

Fig. 4 Current–voltage characteristics of the NT-DSSC devices fabricated using the anodic TNT films with tube lengths (L/μm) of 15 (■), 20 (●), 32 (▲), 43 (▼), and 57 (◆). (a) and (b) show the results without and with $TiCl_4$ post-treatment, respectively, under simulated AM 1.5 solar illumination at 100 mW cm^{-2} with an active area of 0.25 cm^2.

without and with $TiCl_4$ post-treatment, respectively. The truncation feature (<500 nm) and the band structures (>500 nm) shown in all IPCE spectra are due to absorption of the iodide/triiodide electrolyte and the light scattering of the Pt-ITO counter electrode, respectively, for devices in a backside illumination geometry. Integrating the IPCE at each wavelength over the AM-1.5 solar spectrum yields a calculated J_{SC} similar to the collected value for all devices under investigation (Fig. S5, ESI), confirming the results obtained from the corresponding *I*–*V* measurements (Fig. 4).

The IPCE spectra systematically broadened with tube length increasing from L = 15 μm to L = 57 μm. For the tubes without

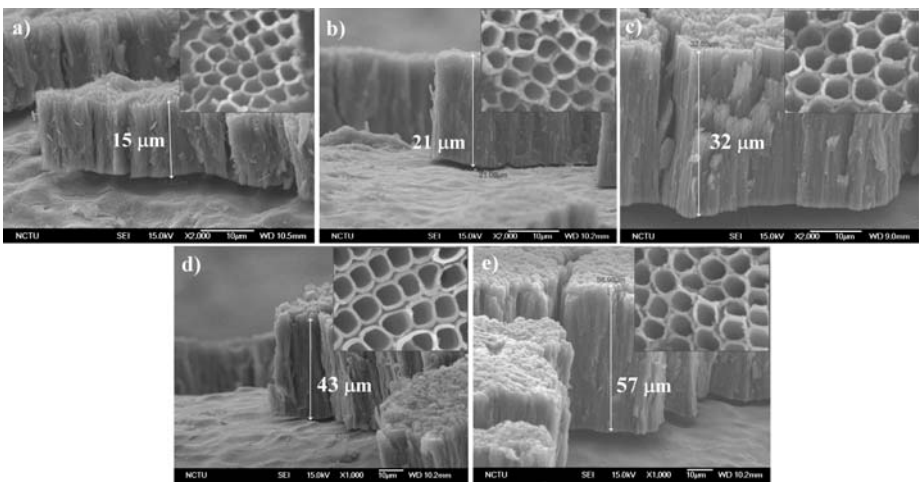

Fig. 3 SEM side-view images of the TNT arrays produced with hybrid anodization periods (*t*/h) (a) 1.5, (b) 2, (c) 3, (d) 4 and (e) 5 at the constant current density 5.6 mA cm^{-2}. The insets, the corresponding SEM top-view images of the TNT arrays, show the average pore diameters/nm (a) 90, (b) 100, (c) 120, (d) 120 and (e) 120.

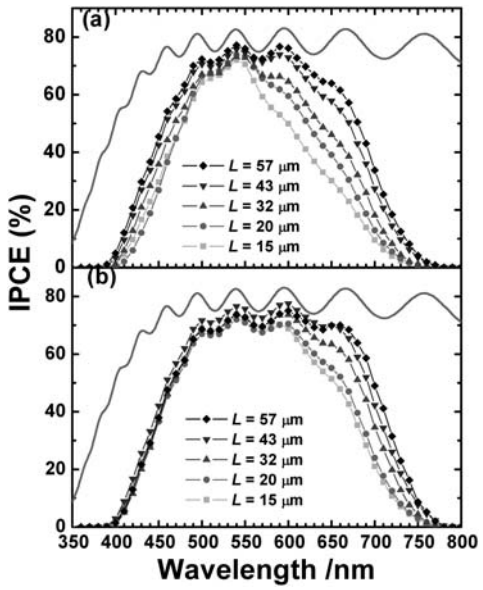

Fig. 5 Corresponding IPCE action spectra of the same NT-DSSC devices as those shown in Fig. 4. The gray curve shows the transmittance spectrum of the Pt/ITO counter electrode for comparison.

$TiCl_4$ treatment, the maximum value of IPCE at 540 nm already attained 72% at $L = 15$ μm. Increasing the tube length increased the maximum IPCE only slightly to 77% but the spectra became significantly broadened, in particular toward the long-wavelength region. With $TiCl_4$ treatment, the IPCE spectra at $\lambda <$ 600 nm are similar for all tubes, but the spectral broadening became more pronounced at $\lambda >$ 600 nm with increasing tube length. The IPCE spectrum of the device with $L = 43$ μm closely follows the transmittance spectrum of the platinized-counter electrode (Fig. 5b) in the wavelength region 500–650 nm with the internal quantum efficiency approaching 90–95% in that region; beyond 650 nm, IPCE decreases rapidly to the background level at ~780 nm but still exhibits a systematic increased trend for the tube length increasing from 15 μm to 57 μm. The increased spectral broadening with increased tube length indicates the light-scattering property of the NT-DSSC devices that harvest more sunlight toward longer wavelength for devices with long TNT arrays. For a NP-based DSSC, a scattering layer of thickness ~ 4 μm (particle size ~ 400 nm) is required to harvest increased light towards longer wavelength;[2–6] the thickness of the active TiO_2 layer is typically restricted to <15 μm[26,27] due to its poorer efficiency of charge collection than the TNT arrays.[20] In contrast, we have demonstrated that the light-scattering effect is an intrinsic feature of NT-DSSC devices, and the TNT arrays can be grown to ~60 μm in a short duration (5 h) with satisfactory cell performance.

Best performance of back-illumination DSSC

The disadvantage of the NT-DSSC device with a backside-illumination structure is the substantial loss of light intensity when irradiation goes through the counter electrode and the electrolyte. The photovoltaic results summarized in Table 1 indicate that the performances of the devices with $L = 30$–60 μm are quite similar ($\eta = 6.6$–6.9%), but the device with shorter tube length gives higher V_{OC}, and also it might suffer less from the absorption of electrolyte if a thinner spacer is implemented. We therefore made an attempt to optimize the cell performance for a NT-DSSC device with $L = 30$ μm using a spacer of similar thickness. Fig. 6 shows the best result from such an attempt, for which J_{SC} and FF increased significantly from 13.6 to 14.6 mA cm^{-2} and from 0.67 to 0.70, respectively, leading to the increase of the power conversion efficiency from 6.6% to 7.6% (with $TiCl_4$ treatment), which is unprecedented for a back-illumination DSSC.[13,15,28]

Grätzel and co-workers[28] have reported a NP-based DSSC device with a photoanode made of Ti-metal substrate spin-coated with TiO_2 nanoparticles under back-side illumination for the purpose of flexible photovoltaic applications. In their approach, the cell performance varies as a function of film thickness and the best result ($\eta = 7.2\%$) was obtained at a thickness of 14 μm due to the limited diffusion length of the nanoparticles.[10] In our case, the back-illuminated NT-DSSC device has reached even higher power conversion efficiency ($\eta =$ 7.6%), for which J_{SC} has been improved significantly compared to that of the NP-based device (14.6 *vs.* 13.6 mA cm^{-2}), indicating the superior light-harvesting efficiency of the NT-based DSSC device with longer tubes ($L \sim 30$ μm). Note that longer tubes provide more room for a greater amount of dye-loading (Table 1), which is an important factor to be considered for the enhancement of J_{SC} *via* extending the light harvesting spectral range towards the longer wavelength region. This effect has been unambiguously observed in our IPCE spectra shown in Fig. 5. The control experiments[28] with glass-made photoanodes have also shown that the cell performance of a front-illuminated NP-DSSC device has reached the performance $\eta = 9.9\%$, which is an increase of ~40% compared to that of the back-illuminated counterpart. Similarly, we expect that a front-illuminated NT-DSSC might have the potential to reach a power conversion efficiency further beyond 10% when the drawback of light absorption from the backside components (Pt-coated counter electrode and the I_3^- electrolyte) can be completely eliminated.

Conclusions

The rate of electron transport in traditional dye-sensitized solar cells is limited by the disordered nature of TiO_2 nanoparticles

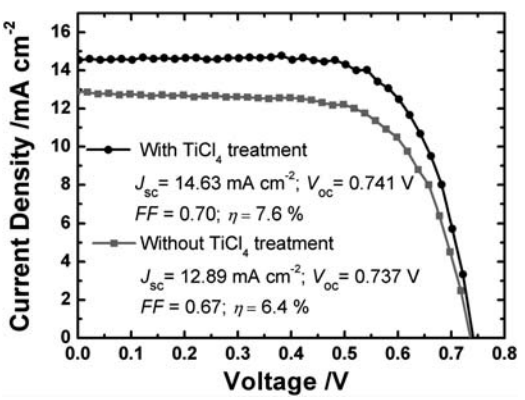

Fig. 6 The cell performances of NT-DSSC devices optimized with $L \sim$ 30 μm using the spacer of the same thickness (30 μm) with or without $TiCl_4$ treatment.

with a small electron diffusion length. To improve the efficiency of charge collection for increased cell performance in a DSSC, vertically aligned TNT arrays have been fabricated using the conventional anodic method at a constant-voltage condition, but the TNT arrays grew slowly due to the current density decreasing during the anodization period. To grow much longer TNT arrays in a much smaller t, we propose a simple hybrid anodic method with initial potentiostatic anodization followed by galvanostatic anodization. The length of the TNT arrays depends linearly on anodization time and is controlled by the electric current; the growth rates are 5.3, 10.7 and 20.3 μm h^{-1} for the applied constant current densities 3.7, 5.6 and 7.5 mA cm^{-2}, respectively. Without $TiCl_4$ treatment, the devices made of TNT films show systematically improved cell performance for tube lengths up to ~60 μm, reflecting the excellent intrinsic light-scattering property of the NT-DSSC devices to harvest increased sunlight with long TNT arrays. With $TiCl_4$ treatment, the cell performance of the device was optimized to reach $\eta = 7.6\%$ at the tube length ~30 μm with a spacer of similar thickness. The great effective surface area inside TNT arrays has the advantage of increasing the amount of dye loading, which might boost the cell performance of the device with co-sensitizing of other dyes for improved efficiency of light harvesting. Our results thus open opportunities to improve further the cell performance for NT-DSSC with multiple dyes co-sensitized in a front-illumination structure.

Acknowledgements

National Science Council of Taiwan and Ministry of Education of Taiwan, under the ATU program, provided support for this project.

References

1 B. O'Regan and M. Grätzel, *Nature*, 1991, **353**, 737.
2 M. K. Nazeeruddin, F. D. Angelis, S. Fantacci, A. Selloni, G. Viscardi, P. Liska, S. Ito, B. Takeru and M. Grätzel, *J. Am. Chem. Soc.*, 2005, **127**, 16835.
3 Y. Chiba, A. Islam, Y. Watanabe, R. Komiya, N. Koide and L. Han, *Jpn. J. Appl. Phys.*, 2006, **45**, L638.
4 F. Gao, Y. Wang, J. Zhang, D. Shi, M. Wang, R. Humphry-Baker, P. Wang, S. M. Zakeeruddin and M. Grätzel, *Chem. Commun.*, 2008, 2635.
5 F. Gao, Y. Wang, D. Shi, J. Zhang, M. Wang, X. Jing, R. Humphry-Baker, P. Wang, S. M. Zakeeruddin and M. Grätzel, *J. Am. Chem. Soc.*, 2008, **130**, 10720.
6 Y. Cao, Y. Bai, Q. Yu, Y. Cheng, S. Liu, D. Shi, F. Cao and P. Wang, *J. Phys. Chem. C*, 2009, **113**, 6290.
7 M. Law, L. E. Greene, J. C. Johnson, R. Saykally and P. Yang, *Nat. Mater.*, 2005, **4**, 455.
8 M. Zukalová, A. Zukal, L. Kavan, M. K. Nazeeruddin, P. Liska and M. Grätzel, *Nano Lett.*, 2005, **5**, 1789.
9 G. K. Mor, K. Shankar, M. Paulose, O. K. Varghese and C. A. Grimes, *Nano Lett.*, 2006, **6**, 215.
10 K. Zhu, N. R. Neale, A. Miedaner and A. J. Frank, *Nano Lett.*, 2007, **7**, 69.
11 G. K. Mor, O. K. Varghese, M. Paulose, K. Shankar and C. A. Grimes, *Sol. Energy Mater. Sol. Cells*, 2006, **90**, 2011, and related references therein.
12 H. Wang, C. T. Yip, K. Y. Cheung, A. B. Djurišić, M. H. Xie, Y. H. Leung and W. K. Chan, *Appl. Phys. Lett.*, 2006, **89**, 023508.
13 K. Shankar, G. K. Mor, H. E. Prakasam, S. Yoriya, M. Paulose, O. K. Varghese and C. A. Grimes, *Nanotechnology*, 2007, **18**, 065707.
14 H. E. Prakasam, K. Shankar, M. Paulose, O. K. Varghese and C. A. Grimes, *J. Phys. Chem. C*, 2007, **111**, 7235.
15 C.-C. Chen, H.-W. Chung, C.-H. Chen, H.-P. Lu, C.-M. Lan, S.-F. Chen, L. Luo, C.-S. Hung and E. W.-G. Diau, *J. Phys. Chem. C*, 2008, **112**, 19151.
16 D. Kim, A. Ghicov and P. Schmuki, *Electrochem. Commun.*, 2008, **10**, 1835.
17 C. C. Chen, W. D. Jehng, L.-L. Li and E. W.-G. Diau, *J. Electrochem. Soc.*, 2009, **156**, C304.
18 J. H. Park, T.-W. Lee and M. G. Kang, *Chem. Commun.*, 2008, 2867.
19 Q. Chen and D. Xu, *J. Phys. Chem. C*, 2009, **113**, 6310.
20 J. R. Jennings, A. Ghicov, L. M. Peter, P. Schmuki and A. B. Walker, *J. Am. Chem. Soc.*, 2008, **130**, 13364.
21 K. Zhu, T. B. Vinzant, N. R. Neale, A. Miedaner and A. Frank, *Nano Lett.*, 2007, **7**, 3739.
22 J. M. Macak, H. Hildebrand, U. Marten-Jahns and P. Schmuki, *J. Electroanal. Chem.*, 2008, **621**, 254.
23 J. Tao, J. Zhao, C. Tang, Y. Kang and Y. Li, *New J. Chem.*, 2008, **32**, 2164.
24 N. Papageorgiou, W. F. Maier and M. Grätzel, *J. Electrochem. Soc.*, 1997, **144**, 876.
25 J. B. Baxter and E. S. Aydil, *Appl. Phys. Lett.*, 2005, **86**, 053114.
26 J. Halmes, G. Boschloo, A. Hagfeldt and P. Lund, *J. Phys. Chem. C*, 2008, **112**, 5623.
27 P. R. F. Barnes, A. Y. Anderson, S. E. Koops, J. R. Durrant and B. C. O'Regan, *J. Phys. Chem. C*, 2009, **113**, 1126.
28 S. Ito, N. C. Ha, G. Rothenberger, P. Liska, P. Comte, S. M. Zakeeruddin, P. Péchy, M. K. Nazeeruddin and M. Grätzel, *Chem. Commun.*, 2006, 4004.

